Analyst

PAPER

View Article Online
View Journal

Cite this: DOI: 10.1039/c5an02633d

Iodine-mediated etching of gold nanorods for plasmonic sensing of dissolved oxygen and salt iodine†

Zhiyang Zhang,[a,b] Zhaopeng Chen,*[a] Fangbin Cheng,[c] Yaowen Zhang[a,b] and Lingxin Chen[a,d]

Received 23rd December 2015,
Accepted 22nd March 2016

DOI: 10.1039/c5an02633d

www.rsc.org/analyst

Here, we have carefully investigated iodine-mediated etching of gold nanorods (AuNRs) in the presence of iodate and applied this phenomenon to on-site detection of dissolved oxygen (DO). Under given conditions, the quantitative conversion of target analytes DO to iodine leads to the etching of AuNRs along the longitudinal direction with the aid of cetyltrimethylammonium. As a result, the longitudinal localized surface plasmon resonance shifts to a short wavelength. The peak-shift can be used for quantitative determination of DO and iodate by a spectrophotometer. The satisfactory results from DO detection in different water samples and iodate detection in table salt indicate the feasibility of the proposed methods. Moreover, the as-prepared colorimetric test paper would make the detection more economical and simpler.

Introduction

Till now, analytical methods for determination of ions and biomolecules have attracted wide concern in environmental and biological analysis.[1–7] Because of the simplicity of the colorimetric method, gold nanoparticles (AuNPs) are now widely employed in colorimetric plasmonic assays based on their strong localized surface plasmon resonance (LSPR) extinction in the visible light region and distance-dependent optical property.[8,9] To date, AuNPs have been used for sensitive detection of various targets, including oligonucleotides,[10,11] proteins,[12,13] metal ions,[14–16] anions[17,18] and some small molecules.[19,20] It is worth noting that the above methods were generally achieved by triggering the aggregation of analyte recognition reagent functionalized AuNPs. These methods need tedious and uncontrollable modification steps. In addition, the nanoparticle-aggregation-based methods also suffer from false positive results due to the autoaggregation.

In contrast, label-free non-aggregation (nanoparticle-etching-based) methods can overcome the above-mentioned problems well.[21–28] These methods are normally based on the shape- and/or size-dependent LSPR property of plasmonic nanostructures,[29,30] highlighted by their tolerance to high salinity (*e.g.*, seawater) and the feasibility to make test paper.[21,24] Unfortunately, this platform, at present, can only be used for detection of very few targets, such as Pb^{2+},[21,22] Cu^{2+},[23,24] Co^{2+},[25] NO_2^-,[26,31] MoO_4^{2-},[32] glucose,[33–35] *etc*. Recently, we demonstrated and certified a clear mechanism for the iodine-induced etching of AuNRs in the presence of cetyltrimethyl ammonium bromide (CTAB) and applied the mechanism to nanoparticle-etching-based sensing. It is worth noting that the proposed etching mechanism is totally different from the iodine-induced transformation of AuNRs mentioned in previous reports.[36–40] So, it is essential to study more about the mechanism and it is also interesting to expand this kind of sensing method.

Dissolved oxygen (DO) is one of the most important indexes in water monitoring, greatly reflecting the degree of water pollution.[41] There are three frequently-used methods for detection of DO, including amperometry (Clark electrode),[42] fluorescence quenching[43] and Winkler's method.[44,45] The Clark electrode is simple, rapid and on-site and has been developed into some commercial products. However, the Clark electrode suffers from aging of the electrode and membrane, which requires frequent and troublesome maintenance. In addition, the Clark electrode can be influenced by phycophyta, sulfide, carbonate and oil because of blocking of the membrane. So, as with

[a]Key Laboratory of Coastal Environmental Processes and Ecological Remediation, Yantai Institute of Coastal Zone Research (YIC), Chinese Academy of Sciences (CAS); Shandong Provincial Key Laboratory of Coastal Environmental Processes, YICCAS, Yantai Shandong 264003, P. R. China. E-mail: zhpchen@yic.ac.cn
[b]University of Chinese Academy of Sciences, Beijing 100049, China
[c]Ocean school, Yantai University, Yantai 264005, P. R. China
[d]College of Chemistry and Chemical Engineering, Yantai University, Yantai 264005, China

†Electronic supplementary information (ESI) available. See DOI: 10.1039/c5an02633d

other electrochemical methods, the stability of the Clark electrode is not so good. Fluorescence quenching methods usually have high sensitivity and fast response, but they need complicated instruments and the fluorescence quenching and the stability of organic molecules can be influenced by many factors, such as pH and temperature. Winkler's method (iodimetry) is a more reliable and cheap method which has been widely used in environmental monitoring. Winkler's method exhibits greater accuracy (0.1%) than other commonly used techniques with an accuracy of 3–5%.[46] Due to its high reliability, Winkler's method is selected as the international standard method for determination of DO (ISO 5813:1983) and it is also the standard method in China (GB7489-87). The only drawback of Winkler's method is the time-consuming titration of iodine in the laboratory which thus restricts the on-site detection of DO for practical application. Therefore, it is essential to modify this assay for use as an on-site method.

As mentioned in the first paragraph, even though a lot of plasmonic assays have been achieved to detect various targets due to their simplicity and sensitivity, a plasmonic assay for DO has never been reported. The possible reason is that the present nanoparticle-aggregation-based assay often needs an appropriate recognition reagent to functionalize AuNPs while a recognition reagent for DO has not been invented so far. Therefore, it interesting and meaningful to make up for the vacancy in the plasmonic sensing method. Our group has been working on the nanoparticle-etching-based assay for some years.[23–26,31,32] One of the advantages of this assay is that it is free of nanoparticle labelling. Inspired by this, here, we develop a label-free plasmonic assay for on-site detection of DO based on the rapid titration of produced iodine using AuNRs as the indicator. The iodine transformed by DO etch (oxidize) AuNRs in the presence of CTAB and results in the blue-shift of longitudinal LSPR of AuNRs accompanied by an obvious color change from blue to red. The shift of longitudinal LSPR has a linear relationship with iodine (or DO) concentration. Since it is not easy to quantify oxygen directly, we use KIO_3 as a substitute for O_2 according to the charge conservation law and iodine produced by the reaction of KIO_3 and KI is used to make a calibration curve.[41] Using this calibration curve, we have achieved DO detection in different water samples as well as the iodate detection in table salt (salt iodine).

Experimental section

Chemicals and apparatus

Hydrogen tetrachloroaurate(III) dehydrate, Cetyltrimethyl Ammonium Bromide (CTAB), ascorbic acid (AA), $NaBH_4$, $NaHCO_3$, $AgNO_3$, KIO_3 and KI were obtained from Sinopharm Chemical Reagent (China). All other chemicals were of analytical reagent grade or better. Solutions were prepared with deionized water (18.2 MΩ, Pall® Cascada). Transmission electron microscopy (TEM) analyses were performed on a JEM-1230 electron microscope (Japan) operating at 100 kV. ESI-MS were determined on a LCQ Fleet ion trap mass spectrometer (Thermo Fisher Scientific, San Jose, USA). The AuNRs were characterized by X-ray powder diffraction (XRD, Rigaku D/Max-2550 pc with Cu Kα radiation) UV/Vis extinction spectra were measured on a Thermo Scientific NanoDrop 2000/2000C spectrophotometer.

Preparation and characterization of gold nanorods

The AuNRs were synthesized using a modified method by changing the amount of $AgNO_3$ (experimental detail is shown in ESI†).[47] The synthesized CTAB-stabilized AuNRs possess an average aspect ratio of 2 : 1 (Fig. 1A). The obtained AuNRs were centrifuged twice at 7500 rpm for 15 min to remove excess CTAB. The obtained soft sediment was re-suspended in deionized water and kept at room temperature. The colloid was found to be stable for at least 6 months. The prepared AuNRs were characterized by both TEM and XRD. The XRD spectrum of AuNRs has a similar pattern with another report and the peak positions are consistent with metallic gold (Fig. S9†).[48]

Procedure for making test paper

Briefly, 5.0 μl of CTAB stabilized GNR colloids was dropped to a specific zone on filter papers (Supor 450, 0.45μm, Pall Corporation, USA). The solution thereafter was evaporated in air sufficiently.

Procedure for detection of KIO_3

The measurement was carried out in a 50 mM glycine/HCl buffer solution (850 μL, pH 2.2) containing 1.0 mM CTAB and 1.0 mM KI. To the buffer solution, 10 μL of KIO_3 with different concentrations and the prepared AuNR (150 μL, 1.4 nM) solution were added in sequence. After incubation at 50 °C for 15 min, the extinction spectra of the mixed solutions were recorded.

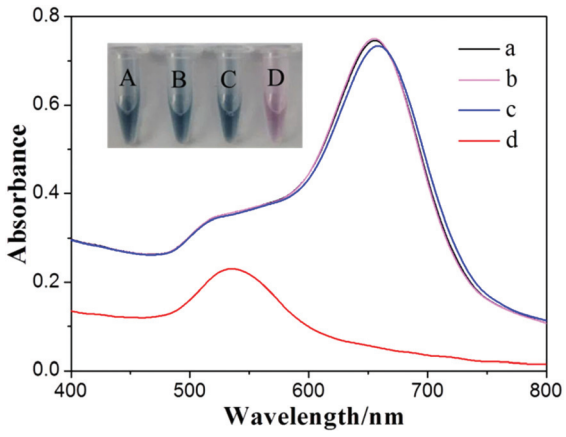

Fig. 1 Extinction spectra and colors of AuNRs in a glycine/HCl buffer solution (a, A) in the presence of 10 μM KIO_3 (b, B), 1.0 mM KI (c, C) and a mixture of 1.0 mM KI and 10 μM KIO_3 (d, D) with incubation at 50 °C for 15 min.

Detection of DO using the modified Winkler's method

(1) Fixing of DO: a mixed solution of 10 μL of $MnCl_2$ (2.1 M) and 10 μL of KI/NaOH (0.9 M KI and 12.5 M NaOH) was added into 2.0 mL samples (seawater, river water and drinking water). The mixed solutions were sealed immediately and then turned upside down for some time. (2) Determination of DO: after sealing for 30 min, 10 μL of the mixed solution was added to a 50 mM glycine/HCl buffer solution (850 μL, pH 2.2) containing 1.0 mM CTAB and 1.0 mM KI. Then, the prepared AuNRs (150 μL, 1.4 nM) were added as the indicator. Finally, the mixed solutions were incubated at 50 °C for 15 min and then the extinction spectra was recorded.

Detection of DO using Winkler's method[44,45]

(1) Fixing of DO: a mixed solution of 1.0 mL of $MnCl_2$ (2.1 M) and 1.0 mL of KI/NaOH (0.9 M KI and 12.5 M NaOH) was added into 100 mL samples (seawater, river water and drinking water). The mixed solutions were sealed immediately and then turned upside down a few times. (2) Determination of DO: after sealing for 60 min, 1.0 mL of Starch (0.5%) was added into the mixed solution and the solution became blue. Then, $Na_2S_2O_3$ (0.01 M) was used for titration of iodine. Finally, the concentration of DO was calculated by the consumption of $Na_2S_2O_3$.

Procedure for detection of iodate in table salt

1.0 g of table salt was dissolved into 5 mL of water. Then, 100 μL of the solution was added to a 750 μL glycine/HCl buffer solution (pH 2.2). Finally, the same procedure was conducted as the procedure for the detection of KIO_3.

Results and discussion

Scheme for detection of DO

Scheme 1 illustrates the detection mechanism of the modified Winkler's method based on iodine-mediated etching of AuNRs. Mn(II) was first added to the sample and precipitated by an alkaline-iodide reagent and was immediately oxidized into Mn(III) and (IV) by dissolved oxygen. After acidification, Mn(III) and (IV) then oxidized iodide into iodine. The produced iodine then etches AuNRs in the presence of CTAB and results in a blue-shift of the longitudinal LSPR absorption of AuNRs. The shift of longitudinal LSPR could be used for quantification of DO.

To simplify the experiment, we also use KIO_3 as a substitution for DO and iodine produced by the reaction of KIO_3 and KI is used to make a calibration curve.[41] According to the charge conservation law, one mole of iodate is equivalent to 3/2 moles of DO in samples. Therefore, the first step in this work is to study the detection of iodate using iodine-mediated etching of AuNRs.

Iodine-mediated etching of AuNRs for detection of iodate

The production of iodine from the reaction between iodate and iodide (I^-) has been applied for the determination of iodate (IO_3^-).[49,50] As a moderate oxidant, iodine also can oxidize CTAB-stabilized AuNRs. Scheme 2 illustrates the sensing mechanism for the detection of iodate. In a glycine/HCl buffer (pH 2.2), CTAB stabilized AuNRs with an aspect ratio of 2 : 1 (Fig. 1A) appeared light blue (photo *a* in Fig. 1) because the absorption around 665 nm was stronger than that around 520 nm (curve a in Fig. 1). The two absorption peaks are assigned to the longitudinal mode and transversal mode of localized surface plasmon resonance (LSPR), respectively.[30] The separate addition of IO_3^- and I^- into the glycine/HCl buffer containing AuNRs induced negligible changes in color (photo *b* and *c* in Fig. 1), longitudinal bands (curve b and curve c in Fig. 1) and an aspect ratio (Fig. 2A–C) of AuNRs, indicating neither IO_3^- nor I^- could etch the AuNRs separately. In contrast, once IO_3^- together with I^- was introduced into the glycine/HCl buffer containing AuNRs, an obvious color change from blue to red (photo *d* in Fig. 1) was observed due to the blue-shift of the longitudinal LSPR from 665 to 565 nm (curve d in Fig. 1). The blue-shift of longitudinal LSPR resulted from the decrease in the aspect ratio (1.2 : 1) of AuNRs (Fig. 2D). We presumed that large amounts of iodine produced from the reaction between IO_3^- and I^- etched AuNRs preferentially along the longitudinal direction, as a result, the average aspect of AuNRs decreased. The asymmetric etching can be attributed to less surface passivation and/or higher reaction activities at the tips of the AuNRs.[51,52]

In the sensing system, there was 1 mM CTAB in the solution. The practical reduction potential of $AuBr_2^-$/Au is calculated to be 0.81 V *vs.* the normal hydrogen electrode (NHE) which is less than that of IO_3^-/I^- (0.95 V *vs.* NHE) at pH 2.2. Theoretically, IO_3^- can directly oxidize AuNRs in the presence of CTAB. However, actually almost no oxidation was observed when IO_3^- was directed added to CTAB-stabilized AuNRs (curve b in Fig. 1). The result indicated that the reaction

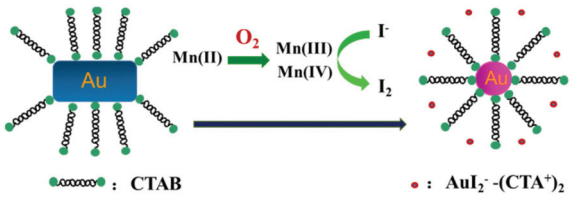

Scheme 1 Scheme for iodine-mediated etching of gold nanorods for plasmonic detection of DO.

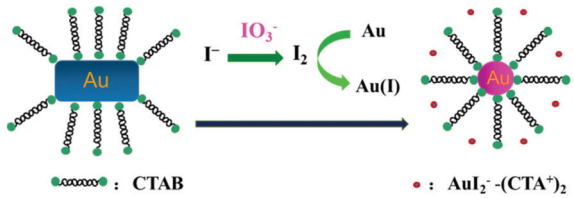

Scheme 2 Scheme for colorimetric sensing of iodate based on iodine-mediated etching of AuNRs.

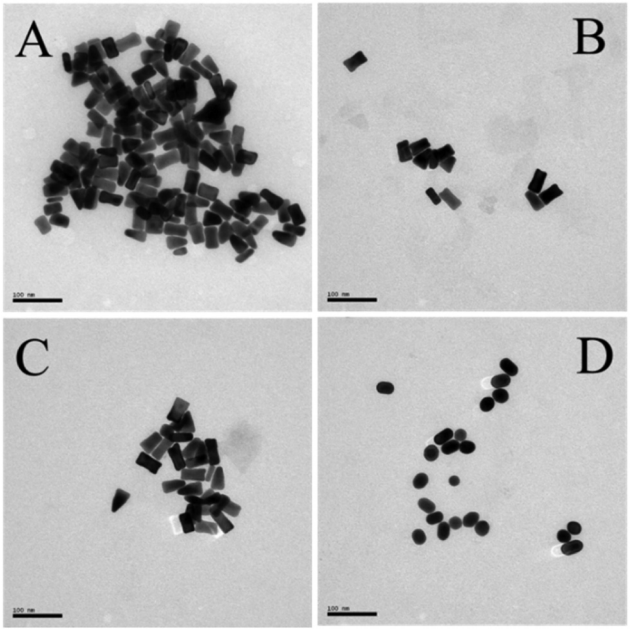

Fig. 2 TEM images of AuNRs in a glycine/HCl buffer solution (A) in the presence of 10 μM KIO_3 (B), 1.0 mM KI (C) and a mixture of 1.0 mM KI and 10 μM KIO_3 (D) with incubation at 50 °C for 15 min.

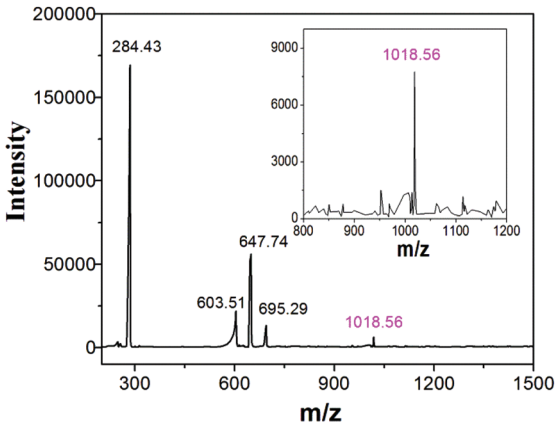

Fig. 3 Mass spectrum of AuNRs solution after incubation with 2.5 mM IO_3^- in glycine/HCl buffer solution containing 10 mM of CTAB, 1.0 mM of I^-.

between IO_3^- and gold was very slow. In contrast, IO_3^- can quickly react with I^- to produce I_2 which was reported to oxidize AuNRs to Au(I) in the presence of CTAB.[32] Therefore, the following reactions were presumed for the etching of AuNRs:

$$IO_3^- + 5I^- + 6H^+ \rightarrow 3I_2 + 3H_2O \quad (1)$$

$$I_2 + I^- \rightarrow I_3^- \quad (2)$$

$$2Au + I_3^- + I^- + 4CTA^+ \rightarrow 2AuI_2^- - (CTA^+)_2 \quad (3)$$

To test the assumption proposed above, firstly, extinction spectra of the reaction product of IO_3^- and I^- were measured to certify the reactions (1) and (2). Fig. S1 (ESI†) shows the UV-vis spectra and color of the glycine/HCl buffer (pH 2.2) containing different reagents, including I^-, IO_3^-, and starch after incubation at 50 °C for 15 min. 1.0 mM I^- did not produce any typical absorption in a range from 200 to 800 nm and the solution appears colorless (curve a and photo a in Fig. S1†). The further addition of 1.0 mM IO_3^- led to an obvious absorption peak at 290 nm and 360 nm accompanied by a color change from colorless to yellow (curve b and photo b in Fig. S1†), indicating that large amounts of I_3^- were produced. The production of iodine was further confirmed by the color change from yellow to dark blue after the addition of starch into the obtained yellow solution. The broad absorption in the range of 400–800 nm (curve c and photo c in Fig. S1†) is attributed to the complex of I_3^- with starch.

To identify the etching product, we added high concentrations (20, 30, 50 μM) of IO_3^- into the AuNR solution in the presence of 1.0 mM KI. Fig. S2 in ESI† shows the colors and extinction spectra of the final solutions. After incubation at 50 °C for 15 min, the solution turned colorless or yellow (photos in Fig. S2†) and the typical absorption peaks of AuNRs at 520 and 665 nm disappeared, indicating that the AuNRs were completely oxidized. The peaks at 290 nm and 360 nm should be assigned to the production of I_3^-,[53] which were consistent to the absorption spectra of I_3^- in Fig. S1 (ESI†). No characteristic absorption peaks at 260, 390 and 400 nm for $AuBr_4^-$ and $AuBr_4^-$-$(CTA^+)_2$ [54–56] were observed in the range from 200 to 800 nm, indicating AuNRs were probably oxidized to Au(I) instead of Au(III). On the other hand, the production of Au(I) is also reasonable in principle. Assuming that Au(III) was produced, Au(III) would be finally reduced into Au(I) anyway by iodide under acidic conditions.[57]

To further prove the etching mechanism, the mass spectrum of the etching product was measured (experimental detail is shown in the ESI†). As shown in Fig. 3, the mass spectrum shows that several components are present: CTA^+ at *m*/*z* 284.43, Cl^-–$(CTA^+)_2$ at *m*/*z* 603.51, Br^-–$(CTA^+)_2$ at *m*/*z* 647.74, I^-–$(CTA^+)_2$ at *m*/*z* 695.29, and the product AuI_2^-–$(CTA^+)_2$ at *m*/*z* 1018.56. All these experimental results demonstrate that gold was transformed into Au(I) instead of Au(III), as shown in reaction (3).

Sensitivity

As shown in Fig. 1, the obvious color change of AuNRs induced by IO_3^- possibly provides a colorimetric method for sensitive detection of IO_3^-. Under the optimized experimental conditions (1.0 mM, of CTAB, pH 2.2, 1.0 mM, of KI, 50 °C incubation temperature, and a 15 min incubation time, Fig. S3–S7, ESI†), we tested the sensing performance of this method toward IO_3^-. Fig. 4A shows the changes of LSPR absorption with the addition of different concentrations of IO_3^-. The longitudinal LSPR peak of AuNRs shifted to a short wavelength gradually with an increase in IO_3^- concentration. Two linear relationships between peak-shift and the concentration of IO_3^- were obtained. One is from 0.2 to 1.0 μM, the

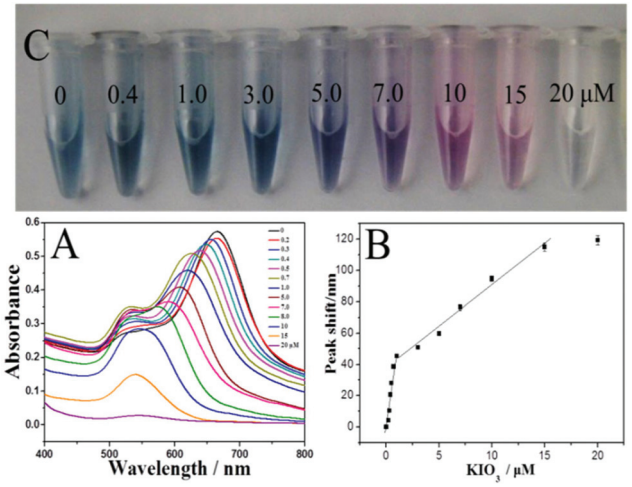

Fig. 4 Extinction spectra (A), LSPR peak-shift (B), and color changes (C) of AuNRs after incubation with different concentrations of IO_3^- at 50 °C for 15 min, respectively.

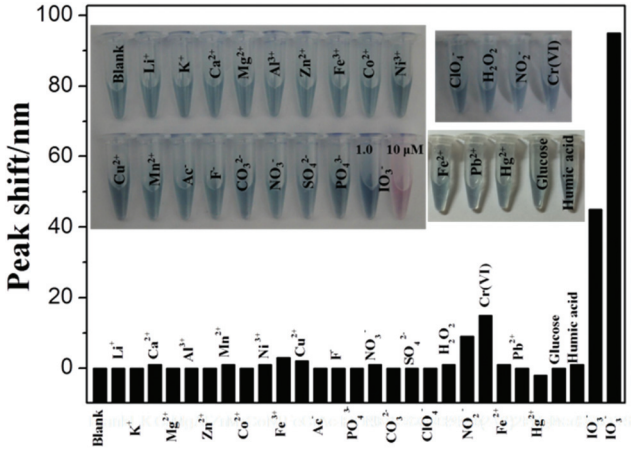

Fig. 5 LSPR peak-shift of AuNRs responding to different ions at different concentrations (1000 μM for Li^+, K^+, Ca^{2+}, Mg^{2+}, Al^{3+}, Ac^-, F^-, CO_3^{2-}, NO_3^-, SO_4^{2-}, PO_4^{3-}; 100 μM for Zn^{2+}, Fe^{3+}, Co^{2+}, Ni^{3+}, Cu^{2+}, Mn^{2+}, Fe^{2+}, Pb^{2+} and glucose; 10 μM for Hg^{2+}, ClO_4^-, and humic acid, 1.0 μM for H_2O_2, NO_2^-, Cr(VI); 1.0 and 10 μM for IO_3^-) in the glycine/HCl buffer solution (pH 2.2) containing 1.0 mM EDTA.

other is from 1.0 to 15 μM (Fig. 4B). The curve slope at a low concentration range (0.2–1.0 μM) is higher than the curve slope at a higher concentration range (1.0–15 μM). This means that the reaction rate at low concentration is faster than that at higher concentration. Two reasons contribute to this phenomenon: (1) the sharp tips at the end of AuNRs have very high reaction activity and make the etching reaction very fast in the beginning. After all the tips were corroded, the reaction rate became slow; (2) the aspect ratio of AuNRs decreases faster in the beginning because the etching almost only happened at the end of AuNRs due to the active tips and then happened at both ends and sides. The longitudinal LSPR therefore changes more quickly along with the changing aspect ratio of AuNRs. Using the relationships, we can directly determine the concentration of iodate in table salt (Table S1, ESI†). The detection limit was calculated to be 0.1 μM (3σ rule), which is comparable with the results obtained by fluorescence spectroscopy, ion chromatography and electrochemistry.[49,50,58–61] The photos in Fig. 4C show the color responses of AuNRs to different concentrations of IO_3^-. Obvious color changes from blue to red then colorless were also obtained with increasing IO_3^- from 0 to 20 μM. Notably, the color change as induced by 3 μM IO_3^- can be directly distinguished by the naked eye.

Selectivity

To test the selectivity of this method toward IO_3^-, various other ions, including Li^+, K^+, Ca^{2+}, Mg^{2+}, Al^{3+}, Zn^{2+}, Fe^{3+}, Co^{2+}, Ni^{3+}, Cu^{2+},Mn^{2+}, Fe^{2+}, Pb^{2+}, Hg^{2+}, Ac^-, F^-, CO_3^{2-}, NO_3^-, SO_4^{2-}, PO_4^{3-}, ClO_4^-, H_2O_2, NO_2^-, Cr(VI), glucose and humic acid were examined. Here, EDTA, a strong chelating agent, was used to decrease the potential interference from metal ions. Fig. 5 shows the peak-shift of longitudinal LSPR in the presence of the above ions with different concentrations. The peak-shift as-induced by 1.0 μM IO_3^- is about 43 nm while 100 μM or 1000 μM of other ions caused a tiny peak-shift. As observed from the photos in Fig. 4, only 10 μM of IO_3^- produced an obvious color response from blue to red, which can be easily observed by the naked eye. The excellent selectivity of this method will greatly benefit the practical applications of the proposed method.

Detection of DO in real water samples

It is necessary to clarify the feasibility of the detection of DO when considering some potential interferences (false positive signal) from NO_2^-, Cr(VI) and H_2O_2. On the one hand, these interferences are negligible when we detect the concentration of DO. In normal water samples, these species usually do not exist at all or exist only at very low concentration levels while DO in water often remains at mM levels. In our methods, the sample is diluted 100 times after formation of iodine and then reacts with AuNRs (experimental part). This means only these species whose concentration is higher than 0.1 mM can produce some interference (because only when the concentration of NO_2^-, Cr(VI) and H_2O_2 is higher than 1.0 μM, the peak shift is obvious as shown in Fig. 4). However, this case is very rare. On the other hand, even if the concentration of these species is higher than 0.1 mM, the interference of these species can be evaluated (using the procedure for detection of iodate) and it can be also subtracted by background correction.

For quantification of DO, the linear relationships between peak-shift and the concentration of IO_3^- were used (Fig. 4B). According to the charge conservation law, one mole of iodate was equivalent to 3/2 moles of DO in samples. The feasibility of the proposed method is evaluated by comparing the determination results obtained from the proposed method and the old Winkler's method. There are two reasons for using the old Winkler's method to validate the proposed method. First, Winkler's method has been reported to exhibit greater

Table 1 Comparison of the proposed method and Winkler's method for detection of DO in real water samples; the standard deviation of each sample was obtained from three measurements

Sample	Proposed method (mg L^{-1})	The Winkler's method (mg L^{-1})
Drinking water	8.2 ± 0.15	8.3 ± 0.23
Lake water	7.4 ± 0.27	7.5 ± 0.13
Sea water	8.0 ± 0.15	7.9 ± 0.18

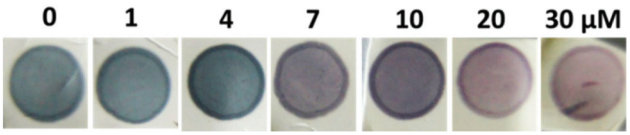

Fig. 6 Photographs of the proposed test paper for the sensing of different concentrations of IO_3^-.

accuracy (0.1%) than other commonly used techniques with an accuracy of 3–5%.[46] Second, the method proposed is actually a modified Winkler's method and the main measuring process is same with the old Winkler's method. So, it should be much more persuasive to use the old Winkler's method for validation. Table 1 shows the detection results in different real samples obtained by the proposed method and Winkler's method. The similar results indicated that the proposed method also possesses high accuracy and stability. In addition, the proposed method can reduce the tedious titration procedure used in Winkler's method, making it possible to be an on-site method. Compared with other nanoparticle-based DO detection techniques (such as the electrochemical method and fluorescence method),[62,63] this method, as a spectrophotometric assay, has better stability and reproducibility. Moreover, it can also be developed into a simple colorimetric method by increasing sampling volume in the determination procedure (experimental part).

Colorimetric sensing using test paper

To further increase its applicability, we explored the feasibility of iodine-mediated etching of AuNRs for colorimetric sensing using test paper.[24] For detection, the test paper was immersed in a 50 mM glycine/HCl buffer solution containing 10 mM CTAB and 1.0 mM KI in the presence of IO_3^-. After incubation at 70 °C for 25 minutes, the color of each test zone was compared. The color turned to red gradually with the increase of IO_3^- (Fig. 6). So, the prepared test paper may be used for semi-quantification of DO. The test paper, as compared to the reported, is much simpler, more economic and more practical for colorimetric sensing.

Conclusions

In our experiment, we investigated iodine-mediated etching of AuNRs in the presence of iodate and apply this to the on-site detection of DO and salt-iodine concentration. The iodine-induced etching mechanism to gold under the assistance of CTA^+ was carefully investigated. The proposed method shows an excellent sensitivity with a detection limit of 0.1 μM and gold selectivity toward iodate. The good analytical performance makes it possible for the successful on-site determination of DO in different waters as well as iodate in table salt samples. Additionally, the colorimetric test paper would make the detection more economical and simpler.

Acknowledgements

The research was financially supported by the Strategic Priority Research Program of the Chinese Academy of Sciences (XDA11020702), the Department of Science and Technology of Shandong Province (BS2009DX006), NSFC (No. 21275158, 21175084, 21275091), CAS (KZCX2-YW-JS208) and the 100 Talents Program of the CAS.

Notes and references

1 H. Zhang, Y. Huang, S. Hu, Q. Huang, C. Wei, W. Zhang, L. Kang, Z. Huang and A. Hao, *J. Mater. Chem. C*, 2015, **3**, 2093–2100.
2 L.-Y. Niu, M.-Y. Jia, P.-Z. Chen, Y.-Z. Chen, Y. Zhang, L.-Z. Wu, C.-F. Duan, C.-H. Tung, Y.-F. Guan and L. Feng, *RSC Adv.*, 2015, **5**, 13042–13045.
3 X. Lin, S.-X. Li and F.-Y. Zheng, *RSC Adv.*, 2016, **6**, 9002–9006.
4 S.-X. Li, X. Lin, F.-Y. Zheng, W. Liang, Y. Zhong and J. Cai, *Anal. Chem.*, 2014, **86**, 7079–7083.
5 Q. Huang, X. Lin, C. Lin, Y. Zhang, S. Hu and C. Wei, *RSC Adv.*, 2015, **5**, 54102–54108.
6 B. Jiang, F. Li, C. Yang, J. Xie, Y. Xiang and R. Yuan, *Anal. Chem.*, 2015, **87**, 3094–3098.
7 Y. Zhang, H. Li, L.-Y. Niu, Q.-Z. Yang, Y.-F. Guan and L. Feng, *Analyst*, 2014, **139**, 3146–3153.
8 K. Saha, S. S. Agasti, C. Kim, X. Li and V. M. Rotello, *Chem. Rev.*, 2012, **112**, 2739–2779.
9 W. Zhou, X. Gao, D. Liu and X. Chen, *Chem. Rev.*, 2015, 10575–10636.
10 R. Elghanian, J. J. Storhoff, R. C. Mucic, R. L. Letsinger and C. A. Mirkin, *Science*, 1997, **277**, 1078–1081.
11 H. Li and L. Rothberg, *Proc. Natl. Acad. Sci. U. S. A.*, 2004, **101**, 14036–14039.
12 H. Wei, B. Li, J. Li, E. Wang and S. Dong, *Chem. Commun.*, 2007, 3735–3737.
13 N. T. K. Thanh and Z. Rosenzweig, *Anal. Chem.*, 2002, **74**, 1624–1628.
14 J. Liu and Y. Lu, *J. Am. Chem. Soc.*, 2003, **125**, 6642–6643.
15 J. S. Lee, M. S. Han and C. A. Mirkin, *Angew. Chem., Int. Ed.*, 2007, **119**, 4171–4174.
16 Z. Zhang, J. Zhang, T. Lou, D. Pan, L. Chen, C. Qu and Z. Chen, *Analyst*, 2012, **137**, 400–405.

17 Z. Zhang, J. Zhang, C. Qu, D. Pan, Z. Chen and L. Chen, *Analyst*, 2012, **137**, 2682–2686.
18 Z. Zhang, Z. Chen, S. Wang, C. Qu and L. Chen, *ACS Appl. Mater. Interfaces*, 2014, **6**, 6300–6307.
19 J. Wang, L. Wang, X. Liu, Z. Liang, S. Song, W. Li, G. Li and C. Fan, *Adv. Mater.*, 2007, **19**, 3943–3946.
20 J. Liu and Y. Lu, *Angew. Chem., Int. Ed.*, 2006, **118**, 96–100.
21 A. R. Ferhan, L. Guo, X. Zhou, P. Chen, S. Hong and D.-H. Kim, *Anal. Chem.*, 2013, **85**, 4094–4099.
22 Y.-Y. Chen, H.-T. Chang, Y.-C. Shiang, Y.-L. Hung, C.-K. Chiang and C.-C. Huang, *Anal. Chem.*, 2009, **81**, 9433–9439.
23 T. Lou, L. Chen, Z. Chen, Y. Wang, L. Chen and J. Li, *ACS Appl. Mater. Interfaces*, 2011, **3**, 4215–4220.
24 Z. Zhang, Z. Chen, C. Qu and L. Chen, *Langmuir*, 2014, **30**, 3625–3630.
25 Z. Zhang, Z. Chen, D. Pan and L. Chen, *Langmuir*, 2014, **31**, 643–650.
26 Z. Chen, Z. Zhang, C. Qu, D. Pan and L. Chen, *Analyst*, 2012, **137**, 5197–5200.
27 Y. Li, Z. Li, Y. Gao, A. Gong, Y. Zhang, N. S. Hosmane, Z. Shen and A. Wu, *Nanoscale*, 2014, **6**, 10631–10637.
28 K. Tan, G. Yang, H. Chen, P. Shen, Y. Huang and Y. Xia, *Biosens. Bioelectron.*, 2014, **59**, 227–232.
29 H. Chen, X. Kou, Z. Yang, W. Ni and J. Wang, *Langmuir*, 2008, **24**, 5233–5237.
30 H. Chen, L. Shao, Q. Li and J. Wang, *Chem. Soc. Rev.*, 2013, **42**, 2679–2724.
31 T. Li, Y. Li, Y. Zhang, C. Dong, Z. Shen and A. Wu, *Analyst*, 2015, **140**, 1076–1081.
32 Z. Zhang, Z. Chen and L. Chen, *Langmuir*, 2015, **31**, 9253–9259.
33 Y. Xia, J. Ye, K. Tan, J. Wang and G. Yang, *Anal. Chem.*, 2013, **85**, 6241–6247.
34 X. Liu, S. Zhang, P. Tan, J. Zhou, Y. Huang, Z. Nie and S. Yao, *Chem. Commun.*, 2013, **49**, 1856–1858.
35 L. Saa, M. Coronado-Puchau, V. Pavlov and L. M. Liz-Marzán, *Nanoscale*, 2014, **6**, 7405–7409.
36 D. K. Smith, N. R. Miller and B. A. Korgel, *Langmuir*, 2009, **25**, 9518–9524.
37 J. Wang, Y. F. Li and C. Z. Huang, *J. Phys. Chem. C*, 2008, **112**, 11691–11695.
38 J. Wang, H. Wu and C. Huang, *Sci. China, Ser. B: Chem.*, 2009, **52**, 188–195.
39 J.-M. Liu, L. Jiao, M.-L. Cui, L.-P. Lin, X.-X. Wang, Z.-Y. Zheng, L.-H. Zhang and S.-L. Jiang, *Sens. Actuators, B*, 2013, **188**, 644–650.
40 J. Zhang, X. Xu, C. Yang, F. Yang and X. Yang, *Anal. Chem.*, 2011, **83**, 3911–3917.
41 S.-C. Pai, G.-C. Gong and K.-K. Liu, *Mar. Chem.*, 1993, **41**, 343–351.
42 J. R. Stetter and J. Li, *Chem. Rev.*, 2008, **108**, 352–366.
43 X.-D. Wang and O. S. Wolfbeis, *Chem. Soc. Rev.*, 2014, **43**, 3666–3761.
44 G. T. Wong and K.-Y. Li, *Mar. Chem.*, 2009, **115**, 86–91.
45 B. Horstkotte, J. C. Alonso, M. Miró and V. Cerdà, *Talanta*, 2010, **80**, 1341–1346.
46 J. H. Carpenter, *Limnol. Oceanogr.*, 1965, **10**, 135–140.
47 T. K. Sau and C. J. Murphy, *Langmuir*, 2004, **20**, 6414–6420.
48 M. Samim, C. Prashant, A. Dinda, A. Maitra and I. Arora, *Int. J. Nanomed.*, 2011, **6**, 1825–1831.
49 R. Li, P. Xu, J. Fan, J. Di, Y. Tu and J. Yan, *Anal. Chim. Acta*, 2014, **827**, 80–85.
50 Y. Bichsel and U. Von Gunten, *Anal. Chem.*, 1999, **71**, 34–38.
51 C. K. Tsung, X. Kou, Q. Shi, J. Zhang, M. H. Yeung, J. Wang and G. D. Stucky, *J. Am. Chem. Soc.*, 2006, **128**, 5352–5353.
52 W. Ni, X. Kou, Z. Yang and J. Wang, *ACS Nano*, 2008, **2**, 677–686.
53 M. Hicks and J. M. Gebicki, *Anal. Biochem.*, 1979, **99**, 249–253.
54 L. Elding and A. Groning, *Acta Chem. Scand. Ser. A*, 1978, **32**, 867–877.
55 J. Rodriguez-Fernandez, J. Perez-Juste, P. Mulvaney and L. M. Liz-Marzan, *J. Phys. Chem. B*, 2005, **109**, 14257–14261.
56 S. Anandhakumar, R. Rajaram and J. Mathiyarasu, *Analyst*, 2014, **139**, 3356–3359.
57 L. Elding and L. Olsson, *Inorg. Chem.*, 1982, **21**, 779–784.
58 C.-R. Tang, Z.-H. Su, B.-G. Lin, H.-W. Huang, Y.-L. Zeng, S. Li, H. Huang, Y.-J. Wang, C.-X. Li and G.-L. Shen, *Anal. Chim. Acta*, 2010, **678**, 203–207.
59 Z. Huang, Q. Subhani, Z. Zhu, W. Guo and Y. Zhu, *Food Chem.*, 2013, **139**, 144–148.
60 T.-J. Li, C.-Y. Lin, A. Balamurugan, C.-W. Kung, J.-Y. Wang, C.-W. Hu, C.-C. Wang, P.-Y. Chen, R. Vittal and K.-C. Ho, *Anal. Chim. Acta*, 2012, **737**, 55–63.
61 A. E. Vilian, S.-M. Chen and B.-S. Lou, *Biosens. Bioelectron.*, 2014, **61**, 639–647.
62 L. Hutton, M. E. Newton, P. R. Unwin and J. V. Macpherson, *Anal. Chem.*, 2008, **81**, 1023–1032.
63 C.-S. Chu and Y.-L. Lo, *Sens. Actuators, B*, 2010, **151**, 83–89.